THE ASTROPHYSICAL JOURNAL, Vol. 154, October 1968

A THEORY OF DUST COMETS. I. MODEL AND EQUATIONS

MICHAEL L. FINSON AND RONALD F. PROBSTEIN
Department of Mechanical Engineering, Massachusetts Institute of Technology
Received November 24, 1967

ABSTRACT

A theory based on kinetic and fluid-dynamic concepts is formulated for the head and tail regions of dust comets. Dust particles having a wide distribution of sizes are assumed to be released from the comet nucleus in an essentially continuous manner in time during the period of distinctive cometary phenomena. The dust particles are accelerated radially outward from the nucleus by drag forces due to the expanding gas in the comet head. This interaction is found to occur only in a small inner head region, where gas densities are high and where the gas may be described as a continuum.

In the tail region, the only significant forces assumed to act on the dust particles are solar gravity and pressure of solar radiation. The motion of the dust particles in dust tails is treated as a hypersonic, collision-free flow. Relatively simple expressions are derived for the surface density in such tails By comparison of calculated distributions of surface density with measured distributions of light intensity, it is possible to determine the dust and head-gas emission rates as functions of time, the distribution of dust-particle sizes, and the emission velocity from the inner head region as a function of particle size and time. The theory is also capable of explaining observed non-radial dust-tail orientations.

I. INTRODUCTION

In this study a theory based on kinetic and fluid-dynamic concepts is formulated for the head and tail regions of dust comets. The results of the theory provide a detailed picture of such comets, including previously unexplained tail-angle orientations, detailed density distributions, dust and gas emission rates, and particle-size distributions.

Great variations in physical composition and appearance occur among comets, but the basic features of any comet are the nucleus, the head or coma, and the tail or tails. The nucleus is a small, solid body, rarely seen except through the largest telescopes and appearing then as a starlike point. Roemer (1966) has photographically estimated the radii of most nuclei to be less than 10 km, with many having radii of less than 1 km.

Only in the neighborhood of perihelion (on the order of 1 a.u. from the Sun) is a comet sufficiently heated by the Sun for the distinctive cometary phenomena to occur, and these phenomena last only a few weeks. It is the matter expelled by the nucleus due to the solar heating which goes to form the diffuse head and tail of the comet. Roughly 1 per cent of the total nuclear mass is lost per perihelion passage (Whipple 1963). The emission process is not entirely continuous in time: explosive "spurts" in the emission, at unpredictable times, may also be observed for some comets. In fact, an actual splitting of the nucleus into two or more parts has been reported for thirteen comets, six or possibly eight of which were experiencing their first perihelion passage (Stefanik 1966).

The most commonly accepted concept of the nucleus structure is Whipple's "icy conglomerate" model, wherein the nucleus is said to consist of frozen H_2O, NH_3, CH_4, etc., interspersed with meteoric or metallic material (see Whipple 1963). The model is consistent with the observed quantity and composition of the emitted material. Further, a possible explanation for the splitting of nuclei is offered in terms of thermal stresses. In this regard, the nucleus is not held to be homogeneous in composition but rather of a brittle, layered nature—one which would be subjected to a "thermal shock" on approaching the Sun for the first time (Whipple and Stefanik 1966). Prediction of this structure requires a knowledge of the conditions under which the comet was formed, though detailed information on the manner, composition, and rate of gas and dust deposition under solar heating may assist in the determination of the structure.

The head or coma is roughly spherical and centered about the nucleus. The light intensity from the head region decreases with distance from the nucleus and can usually be detected out to 10^5–10^6 km from the nucleus (see Wurm 1966). Henceforth we shall take this limit of visibility, 10^5–10^6 km, as a typical head diameter. The light intensity often varies as R^{-1} (R is the radial distance from the nucleus), with more rapid decreases sometimes observed in the outer head regions, say, for $R > 20000$ km (Miller 1961).

It would appear that a comet head consists of neutral gas molecules moving radially outward from the nucleus. The resonance bands which have been identified spectroscopically include those of C_2, C_3, CN, CH, OH, NH, and NH_2. These bands are excited by a fluorescence interaction with the continuum solar radiation (see Swings 1965). The C_2 and CN emissions are by far the strongest. We should not, however, conclude that these two molecules are the primary components of comet heads. As has been pointed out by Biermann and Trefftz (1964), C_2 and CN have particularly strong resonance bands in the visible spectrum, and other neutral molecules could be present in even larger amounts and still not be observed. The recent discovery of the auroral lines of atomic oxygen in comet heads reinforces this point, since the low excitation probabilities of these lines require large amounts of oxygen to provide the observed emissions (see Biermann and Trefftz 1964).

Assuming that the appropriate optical thicknesses are small, the observed light intensity should be proportional to the number of emitting molecules along the observer's line of sight. Thus a variation of the light intensity as R^{-1} corresponds to $n_g \propto R^{-2}$, where n_g is the molecular number density. This simple R^{-2} density variation would be satisfied if the molecules have radial velocities constant with R. Near the nucleus ($R \sim 5$ km) of a bright comet the gas density is estimated to be $n_g \sim 10^{12}$–10^{14} molecules cm^{-3}, and in the outer regions (say, $R \approx 5 \times 10^5$ km) $n_g \sim 10^2$–10^4 molecules cm^{-3}.

An estimate of the expansion velocity of the head gas has been made by Bobrovnikoff (1931) from observations of expanding concentric rings or halos in Halley's Comet in 1910. These halos, presumably due to intermittent emission of gas by the nucleus, were observed to expand with velocities of the order of 0.5 km sec^{-1}. Such a velocity would be appropriate for a gas temperature of about 250°–300° K. This is roughly the temperature which the comet nucleus would acquire in radiative equilibrium at a distance of 1 a.u. from the Sun. Studies of the energy balance involved at the surface of the nucleus, taking into account the energy required to vaporize the head-gas material, reradiation from the nucleus, and the possible effects of shielding of the nucleus by the surrounding dust particles, indicate the temperature at the nucleus surface, or that of the gas at the surface, to be of the order of 150°–250° K (Hübner 1965).

We shall discuss the details of certain studies of the gas flows in comet heads below, in connection with the presentation of a model for the head and tail regions of dust comets. Here, however, it should be pointed out that near the nucleus, where $n_g \sim 10^{12}$–10^{14} molecules cm^{-3}, gas mean free paths are $l_g \sim 10$–10^3 cm. Thus a large number of molecular collisions and a continuum-type flow would be expected in this region. In the peripheral region of the head ($R \approx 5 \times 10^5$ km, $n_g \ll 10^2$–10^4 molecules cm^{-3}), mean free paths are $l_g \sim 10^6$–10^8 km, so that the flow there is clearly free molecular. The transition from continuum to free-molecular flow, defined roughly as the distance at which the local mean free path is of the same order as the typical flow length, which in this case would be the radial distance from the nucleus, occurs at a distance $R \sim 10^3$–10^5 km.

There are two types of comet tails, dust tails and plasma tails, and in any particular comet either or both types may be present. About the only similarity is that, for both types, the center or axis of the tail lies in the comet orbit plane. Plasma tails (type I) are long ($\sim 10^7$–10^8 km), narrow ($\sim 10^5$–10^6 km), straight, and oriented nearly along the extended radius vector from the Sun, but lagging the radial direction by about 3°–5°. This direction corresponds approximately to that of the relative-velocity vector between the solar wind and the comet. We note that the solar wind has a velocity ~ 500 km sec^{-1}

radially outward from the Sun, while the comet velocity tangent to its orbit is ~30–60 km sec^{-1}. Spectroscopic measurements of plasma tails indicate that the composition is predominantly CO^+ and, to a lesser extent, N_2^+. Here, again, the existence of other, invisible, ionic components is quite probable, since the CO^+ ion has especially strong emission bands in the visible spectrum (Biermann and Trefftz 1964). Density estimates in these tails are $10–10^3$ ions cm^{-3}, as in the outer head regions. The motions of structural details indicate very high repulsive accelerations, as much as 100–1000 times that of solar gravity. The structure of such a tail is now known to result from a coupling of the solar wind to the cometary ions by means of the interplanetary magnetic field, which produces the high accelerations observed. The narrowness of the plasma tails is due to the confinement by the magnetic fields (see, e.g., Alfvén 1957; Ness and Donn 1966).

Dust tails (type II) are shorter ($\sim 10^7$ km) and broader than plasma tails, are curved, and lag between the extended radius vector from the Sun and the comet's orbit path. They rarely show much structural detail. A continuous spectrum due to reflected sunlight is observed from dust tails, leading to the concept that they are composed of small "dust" particles. Bessel in the 1830's first suggested that these particles are repelled into the tail by the pressure of solar radiation, the radiation force being of about the same magnitude as that of the solar gravity. Bredichin refined the concept around 1900.

Since the force of radiation pressure is directed radially outward and varies as r^{-2} (r is the distance from the Sun), as does gravity, we may subtract the radiation force from the gravity force and consider the particles to be subject to a smaller, "effective" gravity field. This fact permits the use of Keplerian orbit mechanics to determine the motion of the particles. The strength of the radiation pressure is often measured by the ratio of the radiation force to that of gravity, defined by the quantity

$$1 - \mu = F_{\text{rad}}/F_{\text{grav}} . \tag{1}$$

The radiation force is proportional to the solar intensity multiplied by the cross-sectional area of the particle, while the gravity force is proportional to the particle mass. If we assume the dust particles to be spherical, a mass density ρ_d, and a diameter d, and the nature of the light scattering to be independent of particle size, then

$$F_{\text{rad}} = \frac{Q_{\text{pr}}}{c}\left(\frac{E_s}{4\pi r^2}\right)\frac{\pi d^2}{4} , \tag{2a}$$

$$F_{\text{grav}} = \frac{GM_\odot}{r^2}\left(\frac{\rho_d \pi d^3}{6}\right) . \tag{2b}$$

Here E_s is the mean total solar radiation (3.93×10^{26} W), c the speed of light, G the universal gravitational constant, and $M_\odot$ the solar mass. The quantity Q_{pr} is the scattering efficiency for radiation pressure (van de Hulst 1957) and is here taken to be a constant of the order of unity. The exact value of Q_{pr} depends on the nature of the scattering medium, i.e., whether it is a dielectric or absorbing medium. For a dielectric, Q_{pr} may be as low as $\frac{1}{4}$ to $\frac{1}{2}$, while for an absorbing medium for the particle sizes and wavelengths of interest, $Q_{\text{pr}} \approx 1–2$. As we shall show, Q_{pr} does not enter directly in the calculations to be carried out but appears only as a parameter when reducing the results of the calculations to a particle-size distribution.

Under the given assumptions and with the values of the constants noted, it follows that

$$1 - \mu = C(\rho_d d)^{-1} \tag{3}$$

where

$$C = \frac{3Q_{\text{pr}}E_s}{8\pi cGM_\odot} = 1.19 \times 10^{-4} Q_{\text{pr}} \text{ g cm}^{-2} .$$

Thus radiation pressure is more important for smaller particles. This repulsive force has a negligible effect on the motion of the massive comet nucleus itself.

II. SOME RESULTS FROM PREVIOUS STUDIES OF DUST TAILS

To describe comet tails, it is convenient to use the cometocentric coordinates ξ,η of Figure 1. The coordinates ξ and η are in the comet orbit plane, with ξ positive radially outward from the Sun and η directed opposite to the comet's motion along its orbit. Distances from the orbit plane are measured by the third mutually perpendicular coordinate, ζ.

Now we may imagine that particles of the same size (the same value of $1-\mu$; cf. eq. [3]) and therefore subject to the same repulsive force are emitted at different earlier times τ along the comet orbit. Due to the repulsive nature of the radiation pressure, these orbits will generally be hyperbolic. In Figure 1 we have shown the trajectories (orbits) of particles emitted at three earlier times. The locus in the (ξ,η)-plane of the

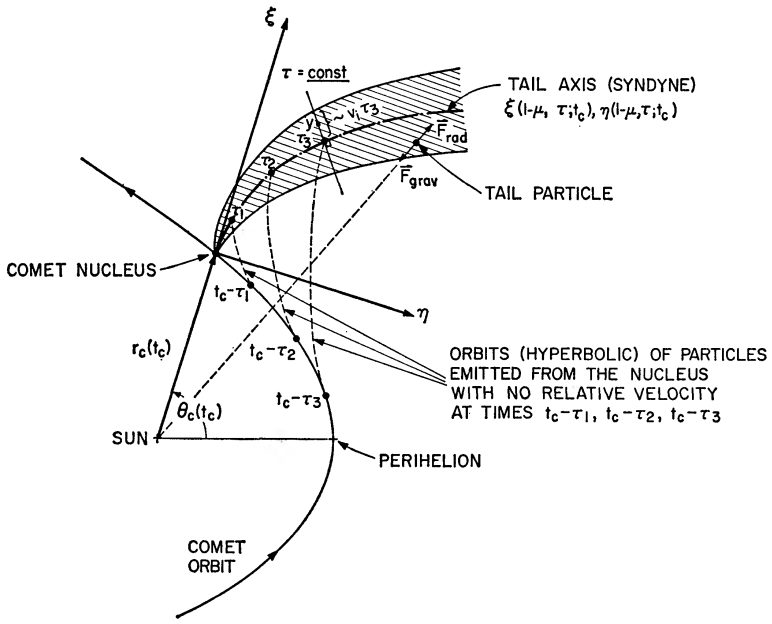

FIG. 1.—Comet tail and particle orbits

positions on these trajectories at the time of observation t_c is termed a "syndyne" (or "syndyname"), to denote particles emitted at different earlier times subjected to the same repulsive force. The syndyne shown in Figure 1 is the locus of particles emitted with zero relative velocity from the nucleus. The time τ is zero at the nucleus ($\xi = \eta = 0$) and increases with increasing distance from the nucleus along the locus. Since the relative emission velocity is zero, the locus must be initially radial, i.e., tangent to the ξ-axis. The curvature in the $+\eta$ direction results from Coriolis effects. A second type of locus, termed a "synchrone," in which all the particles are emitted at the same time (τ = const.) and $1-\mu$ has a wide range of values, will be discussed later.

By comparing observed tail curvatures with the curvatures of calculated syndynes, early investigators were able to estimate values of $1-\mu$, which were found to be typically of the order of 0.1–1.0. Similar values were also deduced from observed accelerations of structural details in the dust tails, although such details are not usually prominent. These values of $1-\mu$ would be appropriate for particle diameters $d \sim 1\ \mu$, assuming $\rho_d \sim 1$ g cm^{-3}.

Information on the emission velocities of the particles from the nucleus is obtained from the observed tail widths (see Fig. 1). If we assume that the nucleus emits dust particles uniformly in all directions with a speed, v_i, the resulting tail will be centered about

the syndyne for zero relative emission velocity, and the tail width at any cross-section will be $\sim 2v_i\tau$. It is this syndyne which is shown in Figure 1 as the tail axis. At a given distance from the nucleus, τ can be determined from the orbit mechanics if $1 - \mu$ is known, and thus v_i can be estimated. Typically, $v_i \sim 1$ km sec^{-1}.

Our knowledge of the dust particles themselves has been greatly expanded by photoelectric and photometric investigations of the two bright comets observed in 1957, Comets Arend-Roland 1956h and Mrkos 1957d, and of Comet Ikeya-Seki 1965f. Liller (1960) photoelectrically measured the continuum light emission from the dust tails of Comets Arend-Roland and Mrkos and found it to be redder than sunlight. He compared the observed energy distribution with theoretical curves for light scattering by small particles, based on the Mie theory. Good agreement was found if the particles were assumed to be iron spheres of 0.6-μ diameter. For these particles Liller calculated a radiation-pressure value, $1 - \mu = 0.13$. From the observed light intensities the average separation of the particles was estimated to be, in Comet Arend-Roland, 4.2 m at a mean distance into the tail of 2.12×10^6 km from the nucleus; in Comet Mrkos, 3.1 m at a mean distance of 4.42×10^6 km into the tail. Using the densities corresponding to these separations and assuming repulsive forces of $1 - \mu = 0.81$ (allowing for additional repulsive forces, suspected at that time, due to the solar wind), the emission rate of dust from the nucleus was then estimated to be $\sim 8 \times 10^7$ g sec^{-1} ($\sim 10^{20}$ particles sec^{-1}) for Comet Arend-Roland and $\sim 10^9$ g sec^{-1} ($\sim 10^{21}$ particles sec^{-1}) for Comet Mrkos.

Remy-Battiau (1964) has analyzed the continuous spectra of reflected sunlight from the head regions of Comets Arend-Roland and Mrkos. Solid dielectric scattering particles with refractive indices between 1.25 and 1.50 and the applicability of the Mie theory were assumed. By comparing a relatively limited number of observational data with calculations for power-law and exponential particle-size distributions, she suggests a size distribution proportional to d^{-4}, with the particles having a refractive index equal to 1.50 and sizes $d \geq 10^{-6}$ cm. Vanýsek (1966) has discussed light scattering by dust particles and also suggests a similar size distribution and refractive index. He points out that, since the particles are presumably very irregular in shape, the Mie theory for spheres may be a poor approximation—a difficulty which Liller (1960) also mentions. From photometric measurements, Vanýsek estimates the total mass of the dust component in the head regions of various comets. For Comet Arend-Roland the value 6.31×10^{11} g of dust was found; for Comet Mrkos, 1.58×10^{11} g. The total number of CN and C_2 molecules in the comet heads was also obtained.

Becklin and Westphal (1966) have made infrared measurements of dust particles in the head region of Comet Ikeya-Seki. From measurements at four different wavelengths, color temperatures were deduced. These were found to be considerably higher than the equilibrium temperature which would be reached by black or gray conducting spheres. Satisfactory agreement was obtained, however, if the emissivity of the dust material was assumed to decrease with increasing wavelengths. Iron, which has this property, was suggested as the likely material.

III. THE DUST-TAIL-ORIENTATION PROBLEM

In the previous section the tail axis was defined as the syndyne for zero relative emission velocity. It was pointed out that such a syndyne leaves the nucleus in the radial direction. A difficulty with this description is that recent observations indicate that dust tails are not directed radially outward from the Sun, even near the nucleus.

The first suggestion of the non-radial nature of comet dust tails was made by Osterbrock (1958), based on observations of the Comets Baade 1954h and Haro-Chavira 1954k. These two comets were observed at rather large heliocentric distances, 3.9–5.0 a.u. No detectable components of a plasma tail were present in either comet. It was found that the tails were located roughly midway between the extended radius vector from the Sun and the orbit path behind the nucleus.

Studies by Belton (1965, 1966*a*) and Brandt and Belton (1966) reveal that the nonradial orientation of dust tails is not a property of distant comets only. An important distinction is raised regarding the simultaneous presence of both dust and plasma tails ("presence" requiring sufficient quantities to be optically or spectroscopically important). Data were compiled for eight comets having prominent dust tails but no detectable plasma tails. All observations of these comets indicated that the initial direction of the dust tails generally lags the radial direction. For three of these eight comets, the Earth passed through the comet orbit plane during the period of observation, and in these instances it was verified that, as had been assumed, the tail axes were indeed located in the orbit plane.

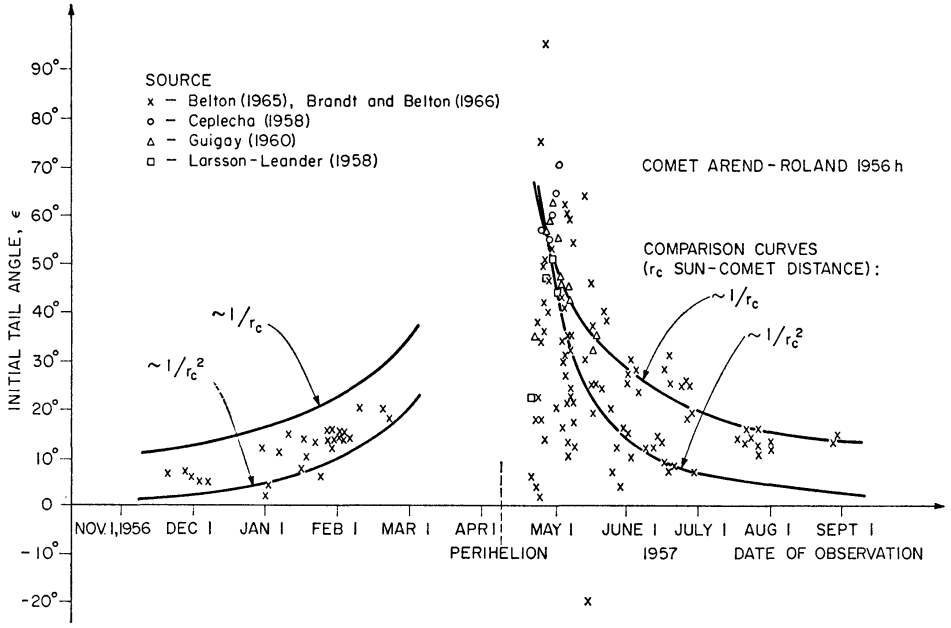

FIG. 2.—Initial tail angle in comet orbit plane as measured from radial direction for Comet Arend-Roland.

On the basis of the observations made by various investigators, Belton (1965) and Brandt and Belton (1966) have tabulated the tail angle, ϵ, in the comet orbit plane for the eight comets considered at various observation times. To avoid possible confusion introduced by the curvature of the dust tails, this angle is taken as the initial tail angle, i.e., the angle between the ξ-axis and the tangent to the tail axis at the comet nucleus, being positive in the $+\eta$ direction. We shall assume that the tail axis is the locus of the apparent maxima in the surface density (or light intensity) in cross-sections normal to the tail. In Figure 2 we have plotted these data for Comet Arend-Roland as a function of the time of observation. We have also included values of ϵ deduced from the isophotes of Ceplecha (1958) and values quoted by Guigay (1960) and Larsson-Leander (1958). The uncertainty in the measured values of ϵ can be traced to the poor projection connected with the Earth's proximity to the comet orbit plane. Also shown for comparison are curves proportional to r_c^{-1} and r_c^{-2}, where r_c is the Sun-comet distance. Figure 3 presents the same data for Comet Van Gent 1941d taken entirely from Belton (1965) and Brandt and Belton (1966). Observations of the other six pure dust comets are less numerous but are certainly not inconsistent with the trends evident in Figures 2 and 3.

In cases where prominent dust and plasma tails are both present (mixed comets), the dust tails usually do not lag the radial direction by the large angles observed for pure

dust comets. Rather, the initial (at the nucleus) orientation of the dust tail appears to coincide with that of the plasma tail, which, as pointed out in § I, lags the radius vector by 3°–5°. In the mixed case, then, there clearly is an important interaction between the dust and plasma components.

From the observational data it is clear that any model of pure dust comets must give tail axes located in the orbit plane, as usual, but at initial angles which may be as much as ~1 radian toward the $+\eta$-axis from the radial direction. The model must also yield angles which vary appropriately with time along the comet orbit.

Let us consider what forces might act on the dust particles that have not already been considered. One possibility is that the dust particles are electrically charged, so that electromagnetic forces must be taken into account. In general, a body situated in a plasma, such as the solar wind, will attain a charge. Various estimates of the charge which the dust particles can attain have been made, the results of which indicate that the dust particles can attain voltages of some tens of volts either positively or negatively

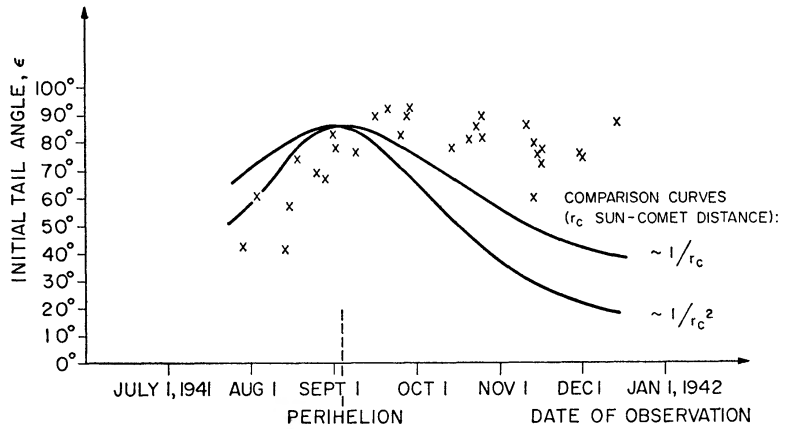

FIG. 3.—Initial tail angle in comet orbit plane as measured from radial direction for Comet Van Gent 1941d. (Data from Belton 1965 and Brandt and Belton 1966)

(Belton 1966*b*; Notni 1966). For a potential of 30 volts, an interplanetary magnetic-field strength $|\boldsymbol{B}| = 5 \times 10^{-5}$ gauss, and a solar-wind velocity $|\boldsymbol{v}| = 500$ km sec^{-1}, the Lorentz force $q(\boldsymbol{v} \times \boldsymbol{B})$ on a dust particle is of the order of 0.1–10 times the radiation-pressure force for particle sizes in the range 0.1–10 μ at a radius of 1 a.u. Most important, however, it is unlikely that a Lorentz force would be properly directed to cause the observed dust-tail orientations. The velocity $\boldsymbol{v}$ is essentially radial, and for $\boldsymbol{v} \times \boldsymbol{B}$ to be in the comet orbit plane and in the $+\eta$ direction, $\boldsymbol{B}$ would have to be perpendicular to the comet orbit plane, in the same sense as the comet's angular momentum. That this could be the case for each of the eight pure dust comets considered by Belton and Brandt is highly unlikely in light of the great variation in the orientations of the different comet orbit planes. In addition, it would be incorrect to conclude even that such forces can be exerted on the particles in a comet dust tail, since the tail as a whole must be electrically neutral. In fact, the Debye length in the solar wind is of the same order as, or less than, the estimated interparticle spacing.

Another possible force could arise from currents (j) being set up in the dust tails, thereby giving rise to $j \times \boldsymbol{B}$ forces. Here, again, however, particular orientations of the magnetic field with respect to the comet orbit plane would be required to give the desired directionality. Various drag interactions with the solar wind, such as Coulomb drag and induction drag, are also possible. These forces are aligned with the relative-velocity vector between the solar wind and the comet, and they can all be shown to be quite small.

On the basis of the arguments given, we may conclude that it is highly unlikely that the orientations of the tails of pure dust comets can be explained by any electromagnetic interactions between the dust particles and the solar wind or the interplanetary magnetic field. Therefore, in what follows we shall neglect any such effects on pure dust tails.

In a preliminary study (Finson and Probstein 1966) a directed, rather than symmetric, emission of dust particles due to asymmetric heating was suggested as a possible reason for the non-radial orientation of the tail. Such an average emission velocity was envisaged in the orbit plane, roughly in the $+\eta$ direction. It should also be pointed out that, in his papers which first proposed the icy-conglomerate model of a comet nucleus, Whipple (1950, 1951) introduced directed emissions (although not always in the $+\eta$ direction) to account for observed small secular changes in the orbital motion of certain short-period comets.

To study the effects of directed emissions, calculations have been made of syndynes for a range of emission velocities in the $+\eta$ direction and for a range of appropriate values of $1 - \mu$. The resulting syndynes were compared with observed orientations and shapes of the tail axis of Comet Arend-Roland. Satisfactory agreement could be obtained only for an emission speed of at least 5 km sec^{-1}. However, such a tangentially directed emission velocity would appear to be unreasonably high. Since the expansion velocity of the head gas is not much greater than 1 km sec^{-1}, velocities of this order could not be achieved except by an explosive event. Not only would this have to occur in a direction tangent to the orbit, but also the duration of the explosion would have to correspond roughly to the period when the comet was in the neighborhood of perihelion. A further difficulty is that no mechanism for the directed emission could be envisioned without requiring a nucleus spin, oriented in a particular manner with respect to the comet orbit plane.

A different treatment of the tail structure has been carried out by Guigay (1960). In his study which was concerned with Comet Arend-Roland, it was assumed that all the dust particles in the comet tail were emitted by the nucleus in one brief burst or explosion, presumably of no more than a day in duration. As mentioned in § I, similar outbursts have been observed in many other comets. Particles of sizes varying over a wide range were assumed to be emitted in a spherically symmetric manner from the nucleus. The observed comet tail then results from the particle-size variations, since the smaller dust particles, for which the effects of radiation pressure are more important (cf. eq. [3]), will be repelled more strongly away from the Sun.

The axis of such a tail corresponds to those particles emitted from the nucleus with no relative velocity, since a symmetric distribution of emission velocities is assumed. Following Guigay, in Figure 4 we show the syndynes in the orbit plane for Comet Arend-Roland on April 27.8, 1957, for zero emission velocity and for several different values of $1 - \mu$. These syndynes are, of course, all initially radial. In Figure 4 we have connected points on the various syndynes with common values of emission time τ. These times are indicated both by dates and in seconds prior to the time of observation ($\tau = 0$ at the time of observation of April 27.8). It is to be noted that perihelion was on April 8.031, corresponding to $\tau = 1.71 \times 10^6$ sec. The different times may be thought of as corresponding to possible times at which a sudden emission of a group of particles of varying size took place. The resulting loci of constant τ, along which $1 - \mu$ varies, are termed "synchrones." Note that, except for the degenerate case $\tau = 0$, synchrones are not tangent to the radial vector, even near the nucleus. Thus, without the need of introducing additional forces or a directed emission, non-radial tail orientations are obtained in a purely kinematic manner if the tail axis is taken to be a synchrone.

Guigay was able to explain an observed tail angle $\epsilon = 46\overset{\circ}{.}5$ on April 25.9, 1957, by assuming that a sudden burst of emission had occurred on or about April 8, the date of the comet's perihelion passage. From the data of Ceplecha (1958) on April 27.8, the

initial tail angle ϵ was observed to be about 50° and the tail length was $\sim 10^7$ km. On Figure 4 we have drawn in this tail orientation. It is clear from the figure that, for the date considered, such a tail would indeed appear to correspond to a synchronic emission on or about April 8 (as may be seen by interpolating between the curves of April 7 and April 10). A difficulty with Guigay's model pointed out by Belton (1965) lies in the orientation of such a synchrone at later dates of observation. The orientation of the synchrone emitted on April 8 has been calculated by the authors to have had an angle $\epsilon = 52°$ on May 3, $\epsilon = 54°$ on May 15, and $\epsilon = 56°$ on July 1. A comparison with the observed values shown in Figure 2 indicates that, although the May 3 value and possibly even the May 15 value are within the observational scatter, the value of 56° on July 1 is not in accord with observations. Belton has also raised a mild objection to the

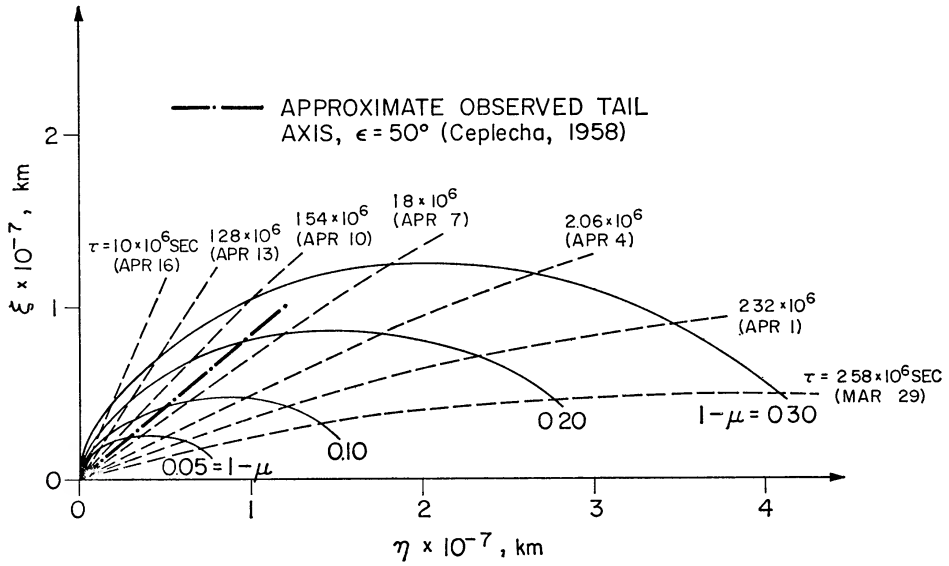

FIG. 4.—Syndynes (*full-line curves*) and synchrones (*dashed-line curves*) for Comet Arend-Roland on April 27.8, 1957 ($\tau = 1.71 \times 10^6$ sec at perihelion on April 8.031).

idea of an emission near perihelion on the grounds that there were no observations of a sudden increase in the brightness of the comet head on or near the date of the assumed emission.

In the next section we present a new model for pure dust comets that appears to be capable of predicting the observed tail orientations and their variation with time. The proposed model is not applicable to comets of mixed type, in which we have seen that near the comet nucleus the orientation of the dust tail coincides with the orientation of the plasma tail, which appears to be the orientation that the plasma tail would assume in the absence of a dust tail. Before presenting our model for the pure dust tail, we would note an explanation for this behavior, proposed by Notni (1966), which appears to be quite reasonable. He has suggested that Coulomb drag forces, discussed earlier in the absence of a plasma tail, arise due to the plasma-tail component acting on the dust particles which are charged. As mentioned in § I, the plasma-tail ions are repelled very strongly from the Sun by an interaction with the solar wind, and Notni assumed, reasonably, that this plasma leaves the head region of the comet with tailward (i.e., nearly radial) velocities of about 10 km sec^{-1}. The resulting Coulomb drag forces on the charged dust particles imparts to them a velocity directed radially outward. This force is strongly dependent on both the plasma properties and the charge of the dust particles.

Neither of these is sufficiently well known for definitive conclusions to be drawn. However, there would appear to be little difficulty with the resolution of the problem of mixed-tail orientation, once more detailed estimates are available for the state of the plasma component, the dust-particle charge, magnetic-field configurations, etc.

IV. MODEL FOR HEAD AND TAIL REGIONS OF DUST COMETS

On the basis of the discussion of the previous section, we shall assume that for pure dust comets no important electromagnetic forces act on the dust particles, so that only the solar gravity and radiation-pressure forces are involved. Thus the original concepts of dust-particle dynamics due to Bessel and Bredichin are retained.

The model proposed is based on the assumption that the dust particles are emitted from the comet nucleus in an essentially continuous manner in time and with a wide distribution of particle sizes. The resultant tail structure at a given time of observation may then be envisaged as resulting from a superposition of a large number of tails of constant particle size (i.e., tails for various values of $1 - \mu$), where the axis of any one constant-particle-size tail is the syndyne for the value of $1 - \mu$ in question. Since all such "syndyne tails" are tangent to the radial direction at the nucleus or coordinate origin, it is not immediately evident how a non-radial tail results from superimposing a large number of syndyne tails. The answer to this important question lies in the shapes of the individual syndyne curves; for illustration we refer to the curves of Figure 4. With reference to this figure, we note in particular the fact that there is a maximum value of ξ for each syndyne and that the values of both ξ and η for which this maximum occurs increase for increasing $1 - \mu$. Now at a given value of η there are very many syndynes for the larger values of $1 - \mu$ (corresponding to the smaller particles) which are near the ξ-axis and which are nearly radial even at relatively large distances from the nucleus. If, however, the contributions to the net density from the lower values of $1 - \mu$, which at that value of η may be close to or already past their maxima, are sufficiently large in comparison with the contributions due to the nearly radial syndynes, then, for distances which can be small in comparison with any resolution length, the tail (a composite of all the "syndyne tails") will be "non-radial."

There is an alternative viewpoint in which the resulting tail can be viewed as arising from a superposition of a large number of "synchrone tails" for different values of the emission time, τ. Except for the degenerate synchrone for $\tau = 0$, none of the synchrones are radial (see Fig. 4). It would appear that such a superposition would therefore give rise to a non-radial tail, in contrast to a radial tail from the superposition of syndyne tails, all of which are tangent to the radial direction at the nucleus. This apparent paradox is resolved by the fact that, as will be shown in the following section, the limiting synchrone tail for $\tau = 0$ is infinitely narrow and tends to make an infinite contribution at the origin to the total density of the tail. At any non-zero distance from the nucleus along this synchrone, $1 - \mu$ has an infinite value. If the relative number of particles approaches zero sufficiently rapidly as $1 - \mu \rightarrow \infty$, the tail may then be non-radial at any non-zero distance from the nucleus. Only at the origin itself must the tail be radial, since $1 - \mu$ will have a finite value for $\tau = 0$, and the same conclusion regarding the non-radiality is reached as above. As will be shown in considering the analysis of the density distribution in the tail, the alternate syndyne and synchrone viewpoints are complementary and lead to the same result.

That the appropriate variation of the tail angle with time should result from the model is suggested by Figure 5. In this figure we have shown the syndynes for $1 - \mu = 0.15$, for various dates of observation for Comet Arend-Roland. If we consider some constant value of ξ close to the nucleus and measure the "non-radiality" by the corresponding values of η for the various syndynes at this value of ξ, we may take these values of η to be a measure of the departure of the tail from the radial direction. It is apparent from this figure that the non-radiality first increases up to the neighborhood of

perihelion (April 8) and decreases at later dates. This behavior, including the rates of departure from and approach to the radial direction as a function of time, is consistent with the trend of the observed tail orientations shown in Figure 2. The syndynes for other values of $1 - \mu$ show a similar behavior, so that the tail for the composite values of $1 - \mu$ should also behave in this manner.

Consistent with equation (3), we take the dust particles to be spherical, of diameter d and density ρ_d, and assume geometric optics to be valid for the particle sizes to be considered, so that $(1 - \mu) \propto (\rho_d d)^{-1}$, where the proportionality coefficient is independent of the particle size. The rate at which dust particles (of all sizes) are emitted from the nucleus will be denoted by $\dot{N}_d(t)$, in particles per second. In the model the distribution of particle sizes is assumed to be constant along the comet orbit, except possibly during an

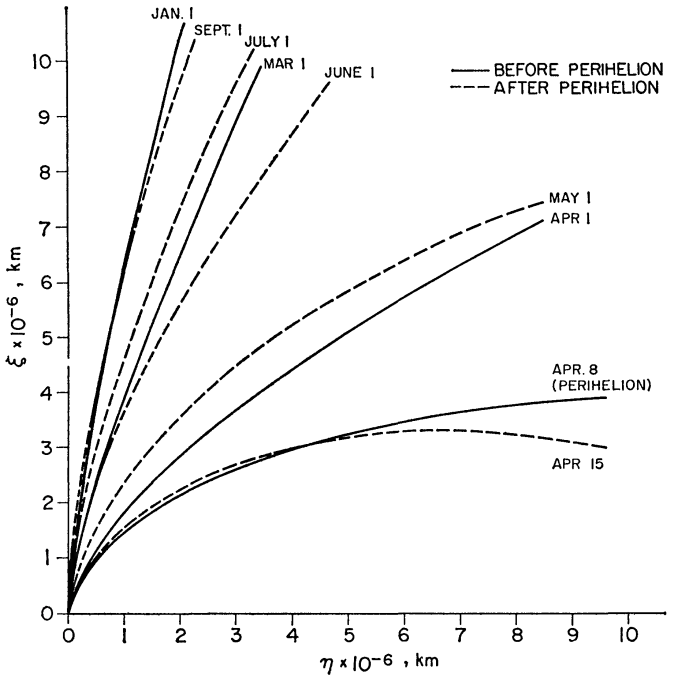

FIG. 5.—Syndynes for $1 - \mu = 0.15$ on various dates of observation for Comet Arend-Roland (all in 1957).

unusual event such as a sudden outburst. It will be convenient to express the distribution of particle sizes in terms of the product $\rho_d d$, which is, of course, expressible in terms of the particle diameter d if ρ_d is assumed constant. We represent this distribution of particle sizes by means of the distribution function $g(\rho_d d)d(\rho_d d)$, defined as the fraction of particles for which $\rho_d d$ is in the range $(\rho_d d)$ to $(\rho_d d) + d(\rho_d d)$. This distribution is normalized to unity by means of the relation

$$\int_0^\infty g(\rho_d d)d(\rho_d d) = 1 \tag{4}$$

where $g(\rho_d d)$ is assumed to be sufficiently well behaved that the integral exists. The quantities $\dot{N}_d(t)$ and $g(\rho_d d)$ are to be regarded as functional parameters to be determined by comparison of calculations based on the model with observation.

To complete the model, a knowledge of the emission velocities of the dust particles from the nucleus is required. For the nature of this emission process we follow the model given in Probstein (1968). In this model the dust particles are assumed to be released

from the nucleus surface with no relative velocity and then accelerated outward as a result of a drag interaction with the expanding head gas. It was found as a result of the interaction that the particles reached a terminal velocity within a distance from the nucleus small in comparison with typical head diameters. Thus the nucleus emission velocities for the tail calculations of the present model are actually seen to correspond to the terminal velocities of the dust particles obtained from the flow solution in the head region.

To understand the solution in the head region, we note that the flow there corresponds to an expanding two-phase "dusty gas." As noted in § I, gas mean free paths in the neighborhood of the nucleus are about 10–10^3 cm and become approximately equal to the radial distance from the nucleus at values of $R = 10^3$–10^5 km. For values of $R < 10^3$–10^5 km, then, the local mean free paths are less than the dimensions of gas flow, so that this flow may be treated from a continuum approach. Since typical gas flow times ($\sim$100 km/ $\frac{1}{2}$ km sec$^{-1} \sim$ 200 sec) are much less than the times over which the comet's orbital position changes ($\sim 10^6$ sec), the flow was considered to be steady. The emission process itself was also taken to be continuous in time, since any changes due to explosive "spurts" would take place on a time scale of the order of a day ($\sim 10^5$ sec).

Since the nucleus is probably rotating on a time scale of the order of 10^4 sec, which is also small in comparison with the time scale over which the comet's orbital position changes ($\sim 10^6$ sec), the nucleus was assumed to be heated symmetrically and the gas-expansion process taken to be spherically symmetric, which is, of course, in accord with the observational facts. The nucleus temperature was assumed to be uniform, and the gas and dust temperatures at the nucleus surface were taken to be the same. No effects of chemical reactions or of heat addition due to the solar radiation were considered in the region of flow. The latter assumption is based on the fact that, while an appreciable amount of solar radiation might be absorbed into internal (electronic, vibrational, and rotational) degrees of freedom of the molecules in the head gas, this energy is reradiated very quickly with little chance of transfer to translational modes. For example, molecules such as C_2 or CN reside in electronically excited states on the order of 10^{-6}–10^{-7} sec before spontaneous emission (using oscillator strengths quoted by Wurm 1963), which is negligible compared with collision times (reciprocal collision frequencies) of at least 10^{-3} sec, based on the head-gas densities quoted in § I.

Since the gas mean free paths are always very much larger than the particle sizes, the drag force exerted on the dust particles was based on the free-molecular drag coefficient (and heat-transfer coefficient) for spheres with perfect accommodation, and the dust particles were considered to be of uniform size. Dust-dust collisions were neglected in the head region. Although at the nucleus the dust-dust mean free path may be only slightly larger than the dimensions of the nucleus, at a given point in the flow all the dust particles will have a common velocity and thus will have a small tendency to collide. It was found that the terminal speed of the dust particles was reached within 20 radii of the nucleus (20–100 km). Functionally, this terminal speed, here denoted by v_i (cf. the speed v_i used in the discussion of § II), was found to be expressible in the form

$$\frac{v_i}{(c_p T_{g_0})^{1/2}} = g(\mathfrak{M},\beta) , \tag{5}$$

where

$$\mathfrak{M} = \dot{m}_d/\dot{m}_g , \quad \beta = \tfrac{16}{3}\pi\rho_d dr_0(c_p T_{g_0})^{1/2}/\dot{m}_g .$$

Here $\dot{m}_g$ is the mass flow rate of the neutral gas and $\dot{m}_d$ the mass flow rate of the dust particles (equal to $\dot{N}_d$ times the mass of the dust particles). The quantity r_0 is the radius of the comet nucleus, T_{g_0} the temperature of the head gas at the nucleus, and c_p the

specific heat of this gas. The results as expressed by equation (5) are shown in Figure 6. We note from this figure that the terminal speeds v_i are of the order of the gas sound speed, which is equal to $[(\gamma - 1)c_p T_{g_0}]^{1/2}$, where γ is the gas specific-heat ratio.

On the basis of these results we assume that the dust particles are emitted from the nucleus in a spherically symmetric manner with a unique speed given by the results of Figure 6. We here consider the gas particles as emitted from the nucleus rather than from the periphery of an "inner head region," since the dimension of this inner head region, ~20–100 km, is negligibly small in comparison with both the coma and the tail dimensions. In terms of the parameters of the present problem, we may then write

$$v_i = v_i(\rho_d d, \dot{N}_d, \dot{m}_g) , \tag{6}$$

where we assume that T_{g_0} and r_0 are known. For example, if we take the gas temperature at the nucleus $T_{g_0} = 200°$ K and the nucleus radius $r_0 = 5$ km, then, for a dust-particle size $d = 1\ \mu$ and density $\rho_d = 5$ g cm^{-3}, the quantity $\beta \dot{m}_g \approx 2 \times 10^8$ g sec^{-1}. For the

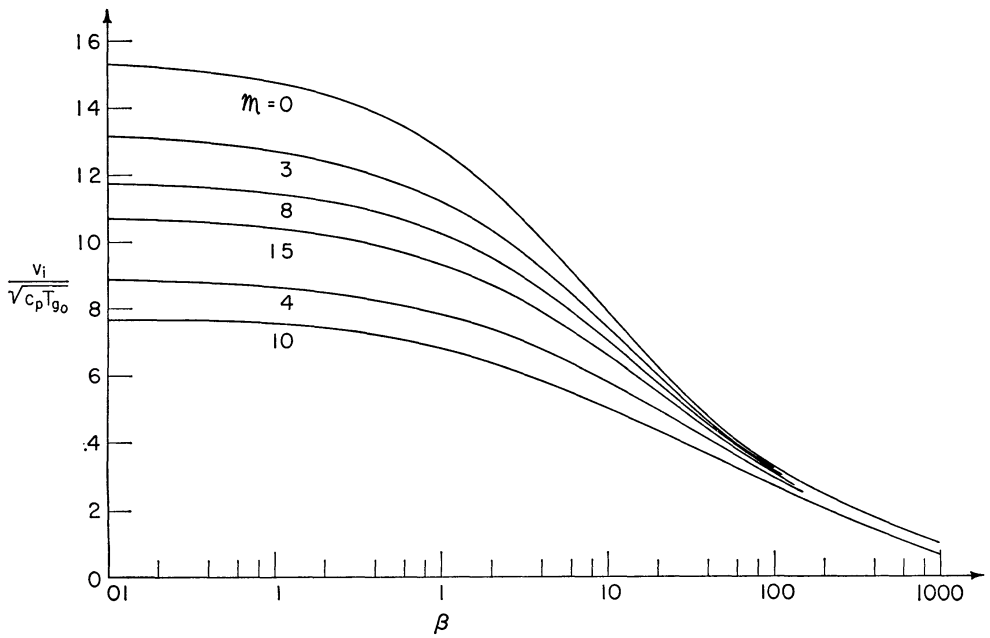

FIG. 6.—Emission speed of dust particles from inner head region (Probstein 1968)

higher gas emission rates estimated by Biermann and Trefftz (1964) of 10^{30}–10^{31} molecules sec^{-1} (with the mass of a gas molecule $\approx 5 \times 10^{-23}$ grams per molecule), we have $\dot{m}_g \sim 5 \times 10^7$ to 5×10^8 g sec^{-1}, and the order of magnitude of the dimensionless parameter β in Figure 6 is seen to be in the range 0.1–10. Of course, the actual values of β may be deduced from v_i, which is one of the quantities to be determined by the present work.

In using the results given in Figure 6, we are neglecting the effects of the variation of particle size as far as the drag interaction in the inner head region is concerned. This assumption is quite reasonable if the particle-size distribution is fairly peaked. In our analysis the mass flow rate of the gas, $\dot{m}_g(t)$, is allowed to vary with time along the comet orbit and, as indicated by equation (6), is a third function (along with $g(\rho_d d)$ and $\dot{N}_d$) that may, in principle, be determined by comparison of theoretically calculated tail shapes and density distributions with the data from dust-tail observations.

In the tail itself, collisions between the dust particles will be neglected. Using the size and spacing estimates of Liller (1960), the dust mean free path in the tail is

$$l_d \sim \frac{1}{n_d \pi d^2} = \frac{1}{(1/4.2 \text{ m})^3 \pi (10^{-4} \text{ cm})^2} \sim 10^{10} \text{ km} , \tag{7}$$

where n_d is the number density of the dust particles.

V. EQUATIONS FOR THE DENSITY DISTRIBUTION IN THE TAIL

Based on the model presented, we now formulate the appropriate equations for calculating the density distribution of the dust in a comet dust tail. As described in the preceding section, our model assumes that the tail of a pure dust comet is at any time an accumulation of particles with a wide range of sizes, emitted by the nucleus over a wide range of previous times. There are two convenient ways to calculate the density in the tail: (1) obtain the density for the tail composed of one particle size (of which the syndyne for the corresponding value of $1 - \mu$ will be the axis), and then integrate tails such as this over all values of $1 - \mu$; or (2) obtain the density for that tail consisting of all the particles emitted at one time (a synchrone will be its axis), and then integrate tails of this type over all values of τ. These two approaches give the same result, since the density involves a double integration (over $1 - \mu$ and τ), and only the order of integration differs. Both approaches are useful in numerical calculations.

Let us illustrate the procedure for the first method, beginning with the derivation of the number-density distribution for a single syndyne tail. Actually, we shall be interested in the integral of the number density along the line of sight from the Earth. This integral is termed the surface density. Because optical thicknesses in dust tails are small, the surface density is proportional to the light intensity, a quantity which can be determined from observations and compared with the theoretically predicted surface density.

Consider the comet to be observed at some time of interest t_c, with $t \equiv 0$ at perihelion. For an individual syndyne tail corresponding to a particular value of $1 - \mu$, the particles are emitted at the time

$$t = t_c - \tau . \tag{8}$$

Here τ is zero at the syndyne origin and increases along the tail axis (see Fig. 1). According to the model described in the previous section, the particles are emitted symmetrically from the nucleus with a speed v_i, which is expressed functionally by equation (6) and given specifically by the curves of Figure 6. We shall assume for the present that the functional parameters which determine this speed, i.e., the particle-size distribution $g(\rho_d d)$, the dust emission rate $\dot{N}_d(t)$, and the head-gas emission rate $\dot{m}_g(t)$, are known or at least have been chosen. Since $\rho_d d \propto (1 - \mu)^{-1}$ from equation (3), then it follows from equations (6) and (8) that we may write

$$v_i = v_i(1 - \mu, \tau; t_c) , \tag{9}$$

where the time of observation t_c is assumed to be fixed and thus a known parameter of the problem.

Now the number of particles emitted in the time τ to $\tau + d\tau$ with sizes in the range $(\rho_d d)$ to $(\rho_d d) + d(\rho_d d)$ is given by

$$\dot{N}_d(t) d\tau g(\rho_d d) d(\rho_d d) , \tag{10}$$

where we note again that t is defined by equation (8), with the time of observation t_c assumed fixed.

For comparison of the calculated densities with observed light intensities, what we are interested in is not the actual particle fraction but this fraction weighted by its light-scattering ability. Now the amount of light scattered is proportional to the cross-sec-

tional area or $(\rho_d d)^2$ for a given ρ_d. In addition, for purposes of calculation it is more convenient to consider $1 - \mu$ rather than $\rho_d d$ as an independent variable. We therefore introduce the weighted distribution function

$$f(1 - \mu)d(1 - \mu) \propto (\rho_d d)^2 g(\rho_d d)d(\rho_d d) . \tag{11}$$

Normalizing this new distribution function to unity,

$$\int_0^\infty f(1 - \mu)d(1 - \mu) = 1 , \tag{12}$$

leads to

$$f(1 - \mu)d(1 - \mu) = (\rho_d d)^2 g(\rho_d d)d(\rho_d d) \Big/ \int_0^\infty (\rho_d d)^2 g(\rho_d d)d(\rho_d d) . \tag{13}$$

Since $1 - \mu = C(\rho_d d)^{-1}$, then

$$f(1 - \mu) = -\frac{1}{C} (\rho_d d)^4 g(\rho_d d) \Big/ \int_0^\infty (\rho_d d)^2 g(\rho_d d)d(\rho_d d) . \tag{14}$$

The number of particles emitted in the time τ to $\tau + d\tau$ in the range $(1 - \mu)$ to $(1 - \mu) + d(1 - \mu)$, weighted by the light-scattering ability of the particles, is therefore

$$\dot{N}_d(t)d\tau f(1 - \mu)d(1 - \mu) . \tag{15}$$

With the particle-size distribution function given, $f(1 - \mu)$ is, of course, determined if the scattering efficiency is known (see eq. [3]). In the present analysis, however, we consider the inverse problem, in which $f(1 - \mu)$ is determined by a comparison of the calculated results with observed light intensities and then the particle-size distribution is found under different assumptions regarding the scattering efficiency.

After emission, this group of particles is repelled tailward by the radiation pressure and simultaneously forms an infinitely thin spherical shell which expands with the speed v_i as expressed by equation (9). The variation of the effective gravity over this shell will tend to warp its spherical shape. However, since the tail widths are of the order of 10^6 km in comparison with heliocentric distances of the order of 10^8 km, this effect is small and will be neglected. At the time of observation, t_c, this group of particles will then form a spherical shell of radius $v_i(1 - \mu, \tau; t_c)\,\tau$, centered at the point on the syndyne locus for the particular value of τ. The syndyne tail is composed of infinitely many such spherical shells, for all possible values of τ from 0 to ∞.

Points on this locus are denoted by ξ_{CM}, η_{CM} (with the subscript "CM" denoting center of mass of the particle groups emitted at the various earlier times $t_c - \tau$) and are calculated using standard Keplerian orbit mechanics, since, as discussed in § II, the particles may be considered to be acted upon by a reduced "effective" gravity as a result of the radiation pressure. In Appendix A the details are given for calculating the position relative to the comet nucleus at the time of observation t_c of a dust particle which is released from the comet nucleus with zero relative velocity at the earlier time $t_c - \tau$ and is acted upon by the reduced effective gravity field. Of course, because of the size of the comet nucleus itself there is no effect on its orbit as a result of the radiation pressure. Since the orbit of the comet nucleus is considered known, the nucleus position and velocity can be found at any desired time along the orbit. The position and velocity of the nucleus at the moment of emission $t_c - \tau$ serve as initial conditions for the particle orbit corresponding to this value of τ with a chosen value of $1 - \mu$. Since the relative emission velocity is taken to be zero, the particle orbits lie within the comet orbit plane. In this case, specification of the resulting particle orbit under the effective gravity field requires the determination of four constants from the known initial conditions at the

time of emission from the source (the comet nucleus). Two constants, say, the semimajor axis and the eccentricity, are required to define the shape and size of the orbit. Since the perihelia of the two orbits (i.e., that of the comet source and that of the particle in question) are not in general aligned, the angle between the perihelia is required as the third constant. And, in general, the comet source and the particle will not reach their respective perihelia simultaneously, so that this time difference becomes the fourth constant. These four constants are determined from the values of the velocity and position (relative to the Sun) at the time of emission. Knowing, then, the orbit of the particle which was emitted at $t_c - \tau$, one can find its position at the later time t_c. This position, relative to the nucleus position at this same time t_c, determines the resulting position on the syndyne axis. The axis may be represented in the parametric form

$$\xi_{CM} = \xi_{CM}(1 - \mu, \tau; t_c) , \quad \eta_{CM} = \eta_{CM}(1 - \mu, \tau; t_c) , \tag{16}$$

with the details of the determination of equations (16) given in Appendix A.

We now must take into account the appearance of such a tail to an observer on the Earth. We define the "plane of the sky" or "photographic plane" as that plane which contains the comet nucleus and is normal to the line joining the nucleus and the Earth. This plane corresponds to photographic plates, and it is desired that points in the comet tail be projected onto this plane. Two coordinates, M and N, are defined in this plane; the M-axis, representing the apparent radial direction, is the projection of the ξ-axis onto this plane. The N-axis is arbitrarily defined to be perpendicular to the M-axis, being chosen so that points on the $+\eta$-axis have positive N values. The geometry and details of the projection of any point ξ,η in the comet orbit plane onto the (M,N)-plane are given in Appendix B.

If we apply the transformation to project the syndyne ξ_{CM},η_{CM} onto the photographic plane, the resulting appearance of the tail axis may be represented in the parametric form

$$M_{CM} = M_{CM}(1 - \mu, \tau; t_c) , \quad N_{CM} = N_{CM}(1 - \mu, \tau; t_c) . \tag{17}$$

Unless the Earth is quite near the comet orbit plane, this locus is qualitatively similar to the ξ_{CM},η_{CM} locus in the comet orbit plane.

In considering the appearance of the previously mentioned spherical shells which expand with the speed v_i, we shall neglect the effects of a finite Earth-comet distance. This is justified on the basis that the radius of such a shell is $\sim 10^6$ km, whereas we shall generally be dealing with Earth-comet distances of $\sim 10^8$ km or greater. Therefore, the distortion in the appearance of a spherical shell due to non-parallel lines of sight connecting various points on the shell is small and may be neglected. Furthermore, the distance along the line of sight between a typical point on the tail axis ξ_{CM},η_{CM} and the photographic plane is generally small compared with the Earth-comet distance. We may therefore assume, with little loss in accuracy, that the spherical shells are centered at the M_{CM},N_{CM} point in the photographic plane rather than at the point ξ_{CM},η_{CM} in the comet orbit plane.

We now seek to determine the modified surface density (i.e., modified so as to be proportional to the light intensity) by carrying out the line-of-sight integration of the density on these spherical shells. A shell of radius $v_i\tau$ is shown in Figure 7, *a*, with the line of sight a distance z_0 from the center. The number of particles on this shell is given by equation (15), so that the number of particles per unit area of the shell surface is obtained by dividing this value by the surface area $4\pi(v_i\tau)^2$. The modified surface density seen by the observer is then

$$2\frac{\dot{N}_d f(1 - \mu)d\tau d(1 - \mu)}{4\pi(v_i\tau)^2}\frac{dA}{dA_\perp} , \tag{18}$$

where dA and $dA_\perp$ are the differential areas shown in Figure 7, *a*, and the factor of 2 takes account of both intersections of the line of sight with the sphere. From the geometry of the figure,

$$\frac{dA_\perp}{dA} = \sin\theta = \left(1 - \frac{z_0^2}{v_i^2\tau^2}\right)^{1/2} \tag{19}$$

so that the modified surface density for such a sphere is

$$\frac{\dot{N}_d f(1-\mu)d\tau d(1-\mu)}{2\pi(v_i\tau)^2[1 - z_0^2/(v_i\tau)^2]^{1/2}}. \tag{20}$$

This result holds, of course, only for $z_0 \leq v_i\tau$, there being no contribution to the surface density for $z_0 > v_i\tau$.

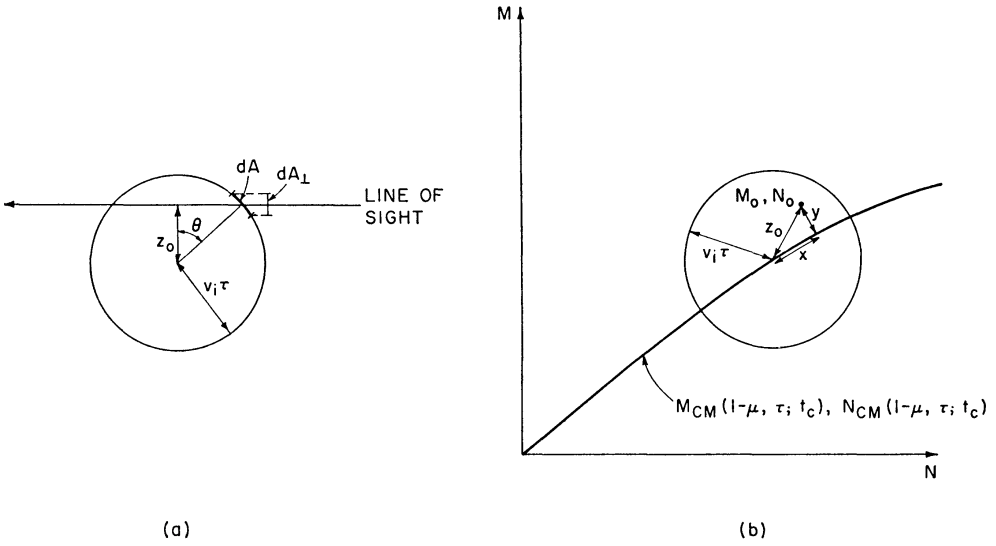

FIG. 7.—Geometry for line-of-sight integration

We now integrate over all such spheres of different τ values for a given line of sight. Figure 7, *b*, shows the M_{CM},N_{CM} axis for a specified value of $1 - \mu$, with a given point of interest M_0,N_0 in the (M,N)-plane located at a normal distance y from the syndyne axis. The line of sight is normal to the (M,N)-plane and intersects it at this point, which is a distance z_0 from the center of any given sphere. The desired surface density is then given by the integral over τ of expression (20):

$$\frac{f(1-\mu)d(1-\mu)}{2\pi} \int_{\tau_1}^{\tau_2} \frac{\dot{N}_d d\tau}{(v_i\tau)^2[1 - z_0^2/(v_i\tau)^2]^{1/2}}, \tag{21}$$

where τ_1 and τ_2 are the values for which $z_0 = v_i\tau$.

In order to simplify the limits of integration and the integral expressed by equation (21), we now introduce a "hypersonic" approximation based on the fact that along a comet tail axis the speed of the particles relative to the nucleus is of the order of 5–20 km sec^{-1}, while the speed v_i with which the particles emanate from the inner head region is of the order of 0.5 km sec^{-1}. We would emphasize that such an approximation greatly facilitates the calculations with negligible loss in accuracy, though it is not necessary

or fundamental to the theory. In the present formulation the hypersonic condition may be expressed as

$$\frac{dx}{d\tau} \gg v_i \,, \tag{22}$$

where $dx/d\tau$ is the rate of change of length along the given syndyne axis with respect to τ (see Fig. 7, *b*). This derivative may be calculated from the results of the orbit mechanics, expressed in functional form by equations (17). Since x represents the length along a syndyne axis, for which $1 - \mu$ is defined to be constant, we have

$$\frac{dx}{d\tau}(\tau; 1-\mu, t_c) = \left[\left(\frac{\partial M_{\rm CM}}{\partial \tau}\right)^2 + \left(\frac{\partial N_{\rm CM}}{\partial \tau}\right)^2\right]^{1/2} . \tag{23}$$

This derivative is a function of τ, which, of course, varies along the syndyne axis, with the selected values of $1 - \mu$ and t_c acting as parameters.

Setting $d\tau = dx/(dx/d\tau)$, the integral of equation (21) may be written

$$\frac{f(1-\mu)d(1-\mu)}{2\pi} \int_{x_1}^{x_2} \frac{\dot{N}_d dx}{(v_i\tau)^2(dx/d\tau)[1 - z_0^2/(v_i\tau)^2]^{1/2}} . \tag{24}$$

The hypersonic condition expressed by equation (22) implies that $dx/d\tau$, the rate of change of length with respect to τ, is so large that the various spheres all have essentially the same value of τ. This, then, enables us to treat $\dot{N}_d$, $v_i\tau$, and $dx/d\tau$ (all of which are functions of τ) as constants over the range of integration. It is here assumed that all these quantities are sufficiently well-behaved functions of τ that they do indeed vary little over the narrow range of τ values involved. Within the hypersonic approximation, equation (24) may thus be written

$$\frac{\dot{N}_d f(1-\mu)d(1-\mu)}{2\pi(v_i\tau)(dx/d\tau)} \int_{x_1}^{x_2} \frac{dx}{[(v_i\tau)^2 - z_0^2]^{1/2}} . \tag{25}$$

If we call the quantity $(dx/d\tau)/v_i$ a speed ratio S, equivalent to a Mach number, then we note that the order of the error in replacing equation (24) by equation (25) is $O(S^{-2})$. This may be seen by expanding $\dot{N}_d$, $v_i\tau$, and $dx/d\tau$ in the integrand (and limits) in equation (24) as a series in ascending powers of the small quantity S^{-2}. The zeroth-order result is then equation (25). This is analogous to the hypersonic approximation in continuum gas dynamics (see, e.g., Hayes and Probstein 1967). It should be pointed out that the expansion assumes all the quantities involved to be well-behaved functions. This may be violated under certain conditions, as, for example, near the origin.

Setting $z_0^2 = x^2 + y^2$, and determining the limits of integration from $(v_i\tau)^2 = z_0^2$ to be

$$x_{1,2} = \pm[(v_i\tau)^2 - y^2]^{1/2} , \tag{26}$$

the integral then reduces to

$$\frac{\dot{N}_d f(1-\mu)d(1-\mu)}{2\pi(v_i\tau)(dx/d\tau)} \int_{x_1}^{x_2} \frac{dx}{[(v_i\tau)^2 - y^2 - x^2]^{1/2}} . \tag{27}$$

With $(v_i\tau)^2 - y^2$ the parameter in the integration over x, the value of the above integral is simply π, so that the modified surface density for an individual (differential) syndyne tail becomes

$$\dot{N}_d f(1-\mu)d(1-\mu)\left[2v_i\tau \frac{dx}{d\tau}(\tau; 1-\mu, t_c)\right]^{-1} . \tag{28}$$

It may be noted that the above result has a simple physical interpretation. The product $\dot{N}_d(t_c - \tau)\, f(1 - \mu)$ gives the number of particles at any point (weighted by their light-scattering ability), while $2v_i\tau$ and $dx/d\tau$ give the dilation in the lateral and longitudinal directions, respectively.

The above solution for an individual differential syndyne tail gives a constant modified surface density across the tail; it applies along a normal to the syndyne axis for a particular value of τ. We note again that equation (28) applies only to points which are actually within the tail. The tail width is $2v_i\tau$, and for points whose normal distance from the axis is greater than $v_i\tau$ the surface density is zero.

To obtain the total modified surface density at a given point M_0,N_0 within the comet tail, we now integrate the different syndyne tails for all values of $1 - \mu$:

$$D = \int_{(1-\mu)_a}^{(1-\mu)_b} \dot{N}_d f(1 - \mu)\left[2v_i\tau \frac{dx}{d\tau}(\tau; 1 - \mu, t_c)\right]^{-1} d(1 - \mu)\,, \tag{29}$$

where $(1 - \mu)_a$ and $(1 - \mu)_b$ are the limiting values of $1 - \mu$ for which the given point lies within the individual syndyne tails. The value of τ in the integrand of equation (29) is related to $1 - \mu$ by the requirement that the point of interest M_0,N_0 lies on a normal to the syndyne axis for each value of $1 - \mu$, i.e.,

$$-\frac{\partial N_{CM}/\partial\tau}{\partial M_{CM}/\partial\tau} = \frac{M_0 - M_{CM}}{N_0 - N_{CM}}\,, \tag{30}$$

with M_{CM},N_{CM} given by equations (17). Since analytic expressions for M_{CM} and N_{CM} are not obtainable in general, further development of the expression for the modified surface density cannot be carried out, and equation (29) must be solved in conjunction with equation (30) numerically.

We shall not derive here the equations for a synchrone tail, since the procedure is completely analogous to that just given, with the roles of $1 - \mu$ and τ reversed. In this case, the hypersonic condition may be expressed as

$$\frac{dx}{d(1 - \mu)} \gg \frac{v_i\tau}{(1 - \mu)}\,. \tag{31}$$

Here we take the relative change of $1 - \mu$ in the distance $v_i\tau$ to be small.

The rate of change of distance along the synchrone axis with respect to $1 - \mu$ is

$$\frac{dx}{d(1 - \mu)}(1 - \mu; \tau, t_c) = \left\{\left[\frac{\partial M_{CM}}{\partial(1 - \mu)}\right]^2 + \left[\frac{\partial N_{CM}}{\partial(1 - \mu)}\right]^2\right\}^{1/2}. \tag{32}$$

The density in an individual (differential) synchrone tail is

$$\dot{N}_d f(1 - \mu)\left[2v_i\tau \frac{dx}{d(1 - \mu)}(1 - \mu; \tau, t_c)\right]^{-1} d\tau\,, \tag{33}$$

which applies at points along the normal to the synchrone axis, whose normal distance from the axis is $\leq v_i\tau$. The value of $1 - \mu$ for the line normal to the synchrone axis for a given value of τ and containing the point of interest M_0,N_0 is found from

$$-\frac{\partial N_{CM}/\partial(1 - \mu)}{\partial M_{CM}/\partial(1 - \mu)} = \frac{M_0 - M_{CM}}{N_0 - N_{CM}}\,. \tag{34}$$

The total modified surface density, D, at a given point is given by

$$D = \int_{\tau_a}^{\tau_b} \dot{N}_d f(1-\mu)\left[2v_i\tau \frac{dx}{d(1-\mu)}(1-\mu;\tau,t_c)\right]^{-1} d\tau \,, \tag{35}$$

where τ_a and τ_b are the limiting values of τ for which the point of interest lies within the individual synchrone tails.

From equation (35) the nature of the limiting synchrone for $\tau = 0$ can now be seen. Not only is τ zero in the denominator of the integrand of equation (35), but the derivative $dx/d(1-\mu)$ also becomes zero at finite x, since $1-\mu$ becomes infinite. Hence, to avoid an infinite contribution to the integrand at $\tau = 0$, $f(1-\mu)$ must decrease sufficiently rapidly as $1-\mu \to \infty$.

The dual, synchrone and syndyne, approaches have been carried out at the risk of some confusion to the reader. The two approaches are, however, useful in actual calculations and their interpretation. The choice of the approach to be used is governed by how well the respective hypersonic conditions, equation (22) or equation (31), are fulfilled.

It is of interest at this point to note the limiting case of $v_i \to 0$, where there is negligible "overlap" of the individual syndyne and synchrone tails, so that the ranges of integration in equation (29) or equation (35) become very small. In this limit, either equation reduces to a simple expression which is independent of the emission velocity v_i and which may be derived easily from either equation. Here, however, we shall use a more direct, physical approach. As above, the modified number of particles in the ranges τ to $\tau + d\tau$ and $(1-\mu)$ to $(1-\mu) + d(1-\mu)$ is given by expression (15). The area occupied by these particles in the plane of the sky, i.e., the (M,N)-plane, is expressed in terms of the Jacobian of the transformation from the M_{CM},N_{CM} to τ, $1-\mu$ values as

$$\left|\frac{\partial M_{CM}}{\partial(1-\mu)}\frac{\partial N_{CM}}{\partial \tau} - \frac{\partial M_{CM}}{\partial \tau}\frac{\partial N_{CM}}{\partial(1-\mu)}\right| d\tau d(1-\mu) \,. \tag{36}$$

The modified surface density is then simply

$$D = \dot{N}_d f(1-\mu)\left(\left|\frac{\partial M_{CM}}{\partial(1-\mu)}\frac{\partial N_{CM}}{\partial \tau} - \frac{\partial M_{CM}}{\partial \tau}\frac{\partial N_{CM}}{\partial(1-\mu)}\right|\right)^{-1} . \tag{37}$$

In practice, it may be expected that this result will be applicable only for very small values of v_i. The resulting comet tail would be essentially two-dimensional, with little extension normal to the comet orbit plane. Such a situation corresponds to the well-known "forward spike" of Comet Arend-Roland, which is thought to consist of particles emitted with exceedingly small values of v_i and which has been observed to be almost perfectly two-dimensional (Öpik 1958; Wurm 1963).

Let us now outline the manner in which data on comets may be deduced by using the results of this section. Here we shall consider the general situation involving, for example, moderate values of v_i, so that equation (29) or equation (35) rather than equation (37) is used to calculate surface densities. Three comet functional parameters are involved in equation (29) or equation (35): $\dot{N}_d(t)$, $f(1-\mu)$, and $v_i(1-\mu, \tau; t_c)$. The first step is then to determine these three functions by matching the calculated and observed light intensities. The procedure for this operation, as well as considerations of uniqueness and sensitivity, is discussed in Paper II of this study, where detailed calculations are presented for Comet Arend-Roland. As long as the absolute level of $\dot{N}_d(t)$ is not required, this first stage involves no assumptions regarding the exact nature of the dust particles, the details of the light scattering from the dust particles, or the precise state of the comet nucleus.

We may distinguish a second stage, where further information can be obtained by

introducing assumptions regarding the light scattering and the dust-particle density. Most important, $1 - \mu$ may be related to the product $\rho_d d$ through equation (3) by assuming a value for the constant $Q_{\rm pr}$. A further choice of ρ_d (assumed uniform over all dust particles) would then yield the particle diameter d. Thus $f(1 - \mu)$ can be related to $g(\rho_d d)$ using equation (14), which in turn could then be expressed in terms of d alone. Similarly, the absolute level of $\dot{N}_d(t)$, which in the first stage was indeterminate by a constant factor involving the amount of light scattered by an individual dust particle, can now be found. Here it is again necessary to relate $1 - \mu$ to d and also to assume a value for the albedo of the dust material. Of course, one can multiply $\dot{N}_d$ by the dust-particle mass, $\rho_d \pi d^3/6$, to obtain the mass production rate of the dust, $\dot{m}_d$. The uncertainty introduced in this stage is probably not high. The scattering efficiency $Q_{\rm pr}$ probably has a value between $\frac{1}{2}$ and 2, while ρ_d is expected to be between 1 and 7 g cm^{-3}. The albedo of the dust particles is less well known, with likely values being between 0.05 and 0.5.

In the third stage the mass production rate of the head gas is determined through Figure 6, with v_i now expressed in terms of $\rho_d d$ and t. At this point, values must be assumed for the nucleus radius r_0, the nucleus temperature T_{g_0}, and the head-gas specific heat c_p. As mentioned in § I, fairly definitive estimates already exist for these quantities. Further, $\dot{m}_g$ can be related to the molecular production rate of the head gas, $\dot{N}_g$, in molecules per second, by assuming a value for the molecular weight of the head gas. It should be pointed out that any uncertainty introduced in the previous two stages will be perpetuated through this stage and compounded by the uncertainties in this third stage.

In Paper II of this study the steps outlined have been carried out for Comet Arend-Roland. It is shown there that the proposed model and theory are capable of providing remarkably accurate comparisons of the calculated distributions of surface density with observed distributions of light intensity. In addition, the previously anomalous non-radial tail orientations and the variation of the tail angle with time are well explained. Other quantities which are shown to be deducible in a unique manner are the distribution of dust-particle sizes, the dust emission rate as a function of time, the head-gas emission rate as a function of time, and the emission velocities from the inner head region as a function of particle size and time.

This work has been sponsored by the Advanced Research Projects Agency (Ballistic Missile Defense Office) and technically administered by the Fluid Dynamics Branch of the Office of Naval Research under contract Nonr-1841(93).

APPENDIX A

ORBIT MECHANICS FOR NUCLEUS AND DUST PARTICLES

We wish to determine the position relative to the comet nucleus, at the time of observation t_c ($t \equiv 0$ at the comet's perihelion), of a dust particle which is released from the comet nucleus at the earlier time $t_c - \tau$ subject to a repulsive force of radiation pressure during the intervening time. The methods of celestial mechanics to be used are described more fully, for example, in Sterne (1960).

As discussed in § I, the dust particles may be considered to be acted upon by a lower effective gravity as a result of the radiation pressure, while this repulsive force has a negligible effect on the motion of the comet nucleus. If r_d is the heliocentric distance of a dust particle, $M_\odot$ the solar mass, and G the gravitational constant, the acceleration of gravity is $-i_R GM_\odot/r_d^2$. With $1 - \mu$ denoting the ratio of the force of radiation pressure to that of gravity, then the effective gravity acceleration is

$$-i_R[1 - (1 - \mu)]\frac{GM_\odot}{r_d^2} = -i_R\frac{\mu GM_\odot}{r_d^2}. \qquad \text{(A1)}$$

In the following, t_c, τ, and $1 - \mu$ or μ are to be considered known, representing particular values of interest.

The dust particle under consideration is taken to be released from the comet nucleus with no relative velocity, so that the ensuing particle orbit will be contained in the comet orbit plane. As in Figure 1, $r_c(t)$ and $\theta_c(t)$ are the heliocentric polar coordinates of the comet nucleus, and $r_d(t)$ and $\theta_d(t)$ are those of the dust particle. The angle θ is taken to be zero at the perihelion of the comet orbit and to increase in the direction of the comet motion. From the geometry of Figure 1, the desired position of the dust particle relative to the comet nucleus at time t_c is

$$\xi = r_d(t_c) \cos [\theta_c(t_c) - \theta_d(t_c)] - r_c(t_c) , \quad \eta = r_d(t_c) \sin [\theta_c(t_c) - \theta_d(t_c)] . \quad \text{(A2)}$$

For concreteness we shall here assume the comet orbit to be parabolic. This is an excellent approximation for most comets and is well satisfied for Comet Arend-Roland, to be discussed in Paper II. Letting q_c denote the (known) perihelion distance, the equation of such an orbit is

$$r_c(t) = 2q_c/[1 + \cos \theta_c(t)] . \quad \text{(A3)}$$

To find $r_c(t)$ and $\theta_c(t)$ for a particular value of t, one first solves the cubic equation

$$\tfrac{1}{3}z^3 + z = \left(\frac{GM_\odot}{2q_c^3}\right)^{1/2} t , \quad \text{(A4)}$$

which has only the one real root

$$z = \left[\tfrac{3}{2}\left(\frac{GM_\odot}{2q_c^3}\right)^{1/2} t + \left(\tfrac{9}{4}\frac{GM_\odot}{2q_c^3} t^2 + 1\right)^{1/2}\right]^{1/3} + \left[\tfrac{3}{2}\left(\frac{GM_\odot}{2q_c^3}\right)^{1/2} t - \left(\tfrac{9}{4}\frac{GM_\odot}{2q_c^3} t^2 + 1\right)^{1/2}\right]^{1/3} . \quad \text{(A5)}$$

Then $r_c(t)$ and $\theta_c(t)$ are given by

$$r_c(t) = q_c(1 + z^2) , \quad \theta_c(t) = 2 \tan^{-1} z . \quad \text{(A6)}$$

Thus the comet position at times such as $t = t_c$ or $t = t_c - \tau$ may be found.

It is now necessary to determine the orbit of the particle from the initial conditions at the time of emission $t_c - \tau$. With a parabolic comet orbit and a non-zero value of the radiation pressure, this orbit will be hyperbolic. Only values of $1 - \mu < 1$ are considered, so that the effective gravity is attractive. This range of values of $1 - \mu$ corresponds to those studied for Comet Arend-Roland in Paper II.

Four constants are required to specify such a particle orbit. Two, such as the semimajor axis a_d and the eccentricity e_d, give the shape of the orbit; the third, α_d, gives the orientation of its perihelion with respect to that of the comet orbit; and the fourth, t_{0d}, is the moment of time at which the particle perihelion is reached. For hyperbolic orbits,

$$a_d < 0 , \quad e_d > 1 , \quad \text{(A7)}$$

and the equation for the orbit path is

$$r_d(t) = \frac{a_d(1 - e_d^2)}{1 + e_d \cos [\theta_d(t) - \alpha_d]} . \quad \text{(A8)}$$

If these orbit constants are known, $r_d(t)$ or $\theta_d(t)$ may be determined by introducing the quantity $F(t)$ defined by the equation

$$\left(\frac{e_d + 1}{e_d - 1}\right)^{1/2} \tanh \frac{F(t)}{2} = \tan \frac{\theta_d(t) - \alpha_d}{2} . \quad \text{(A9)}$$

The quantity $F(t)$ is found from the solution of the transcendental equation

$$e_d \sinh F(t) - F(t) = \left(-\frac{\mu GM_\odot}{a_d^3}\right)^{1/2}(t - t_{0_d}) . \tag{A10}$$

From equation (A8), $r_d(t)$ is found and, in terms of F, becomes

$$r_d(t) = -a_d[e_d \cosh F(t) - 1] . \tag{A11}$$

From equation (A8) or equation (A9), $\theta_d(t)$ can then be found.

To determine the four unknown orbit parameters, we note that at the time of emission the particle and nucleus positions must coincide:

$$r_d(t_c - \tau) = r_c(t_c - \tau) , \quad \theta_d(t_c - \tau) = \theta_c(t_c - \tau) . \tag{A12}$$

Also, at emission, the radial and tangential components of the dust-particle velocity, with respect to the Sun, must equal those of the nucleus. The radial components of the orbital motions are

$$\frac{dr_c(t)}{dt} = \left(\frac{GM_\odot}{2q_c}\right)^{1/2} \sin \theta_c(t) , \quad \frac{dr_d(t)}{dt} = \left[\frac{\mu GM_\odot}{a_d(1 - e_d^2)}\right]^{1/2} e_d \sin [\theta_d(t) - \alpha_d] , \tag{A13}$$

and the tangential components are

$$\frac{d\theta_c(t)}{dt} = (2q_c GM_\odot)^{1/2}/r_c^2(t) , \quad \frac{d\theta_d(t)}{dt} = [\mu GM_\odot a_d(1 - e_d^2)]^{1/2}/r_d^2(t) . \tag{A14}$$

Equations (A12)–(A14), along with equations (A3) and (A8) for r_c and r_d, can be solved for e_d, a_d, and α_d:

$$e_d = \left[1 + \frac{4(1 - \mu)q_c}{\mu^2 r_c(t_c - \tau)}\right]^{1/2} , \tag{A15}$$

$$a_d = -\frac{\mu}{2(1 - \mu)} r_c(t_c - \tau) , \tag{A16}$$

$$\alpha_d = \theta_c(t_c - \tau) - \sin^{-1}\left[\frac{\sin \theta_c(t_c - \tau)}{\mu e_d}\right] . \tag{A17}$$

In the last equation, the arc sine should be taken in the first or fourth quadrant if $\mu r_c/2q_c > 1$, or in the second or third quadrant if $\mu r_c/2q_c < 1$. From equations (A9) and (A10), t_{0_d} is then obtained:

$$F(t_c - \tau) = 2 \tanh^{-1}\left[\left(\frac{e_d - 1}{e_d + 1}\right)^{1/2} \tan \frac{\theta_c(t_c - \tau) - \alpha_d}{2}\right] , \tag{A18}$$

$$t_{0_d} = t_c - \tau - (-a_d^3/\mu GM_\odot)^{1/2}[e_d \sinh F(t_c - \tau) - F(t_c - \tau)] . \tag{A19}$$

Having the four parameters necessary to describe the particle orbit corresponding to the chosen values of t_c, τ, and $1 - \mu$, we may find the particle position at time t_c. Equation (A10) is solved (iteratively) for $F(t_c)$, and equations (A9) and (A11) give $r_d(t_c)$ and $\theta_d(t_c)$. Equations (A2) then give the position relative to the nucleus.

APPENDIX B

PROJECTION BETWEEN ORBIT AND PHOTOGRAPHIC PLANES

In order to determine the appearance of a comet according to an observer stationed on the Earth, the position of the Earth relative to the comet must first be found. Daily values of the Earth's position relative to the Sun are tabulated in *The American Ephemeris and Nautical Almanac* (yearly), the values being given in equatorial coordinates. These values can be related to the cometocentric coordinates of the Earth (ξ_e,η_e,ζ_e) by standard methods (see, e.g., Sterne 1960).

We may now define a cometocentric coordinate system, L,M,N, which is useful for comparison with comet photographs. It will be assumed that the telescopic axis is directed toward the comet nucleus, so that the photographic plate is normal to the line connecting the Earth and the comet nucleus. The error introduced by this assumption is quite negligible if the telescope is directed to within 2°–3° of the nucleus.

The straight line connecting the Earth and the nucleus is given by

$$\frac{\xi}{\xi_e} = \frac{\eta}{\eta_e} = \frac{\zeta}{\zeta_e} . \tag{B1}$$

The L-axis of the L,M,N coordinate system is taken to be along this line and directed toward the Earth. The plane normal to this line and containing the comet nucleus corresponds to the "plane of the sky" or the "photographic plane." It contains the M- and N-axes and is given by

$$\xi_e\xi + \eta_e\eta + \zeta_e\zeta = 0 . \tag{B2}$$

It will be convenient to work with unit vectors. The unit vector along the L-axis is, from equation (B1), in terms of unit vectors along the ξ-, η-, and ζ-axes,

$$\boldsymbol{i}_L = \frac{\xi_e}{\Delta}\boldsymbol{i}_\xi + \frac{\eta_e}{\Delta}\boldsymbol{i}_\eta + \frac{\zeta_e}{\Delta}\boldsymbol{i}_\zeta , \tag{B3}$$

where $\Delta = (\xi_e^2 + \eta_e^2 + \zeta_e^2)^{1/2}$ is the Earth-comet distance. The M-axis is now defined as the apparent radial direction on a photograph, i.e., the projection of the ξ-axis onto the plane determined by equation (B2). This projection is then the line of intersection between this plane and that plane determined by the Earth-comet line and the ξ-axis. Since the normal vector to a plane is given by the vector product of any two (non-parallel) vectors contained in the plane, the vector normal to the latter plane is

$$\pm\boldsymbol{i}_\xi \times \boldsymbol{i}_L = \pm\left(-\frac{\zeta_e}{\Delta}\boldsymbol{i}_\eta + \frac{\eta_e}{\Delta}\boldsymbol{i}_\zeta\right) .$$

The resulting unit vector is

$$\boldsymbol{j} = \pm\frac{-\zeta_e\boldsymbol{i}_\eta + \eta_e\boldsymbol{i}_\zeta}{(\eta_e^2 + \zeta_e^2)^{1/2}} . \tag{B4}$$

Since the vector along the line of intersection between two planes is given by the vector product of the normal vectors of the planes, the unit vector along the M-axis is

$$\boldsymbol{i}_M = \boldsymbol{i}_L \times \boldsymbol{j} = \frac{(\eta_e^2 + \zeta_e^2)^{1/2}}{\Delta}\boldsymbol{i}_\xi - \frac{\xi_e\eta_e}{\Delta(\eta_e^2 + \zeta_e^2)^{1/2}}\boldsymbol{i}_\eta - \frac{\xi_e\zeta_e}{\Delta(\eta_e^2 + \zeta_e^2)^{1/2}}\boldsymbol{i}_\zeta . \tag{B5}$$

The sign of equation (B5) was chosen so that the positive M direction corresponds to increasing ξ (i.e., radially outward).

The third coordinate, N, also lies in the photographic plane and is chosen to form a right-handed set with L and M:

$$i_N = i_L \times i_M \,. \tag{B6}$$

In fact, i_N is identical with j of equation (B4), using the minus sign:

$$i_N = \frac{\zeta_e}{(\eta_e^2 + \zeta_e^2)^{1/2}} i_\eta - \frac{\eta_e}{(\eta_e^2 + \zeta_e^2)^{1/2}} i_\zeta \,. \tag{B7}$$

From equations (B3), (B5), and (B7), we have the desired transformation from the ξ,η,ζ system to the L,M,N system:

$$\begin{aligned} L &= \frac{\xi_e}{\Delta}\xi + \frac{\eta_e}{\Delta}\eta + \frac{\zeta_e}{\Delta}\zeta \,, \\ M &= \frac{(\eta_e^2 + \zeta_e^2)^{1/2}}{\Delta}\xi - \frac{\xi_e\eta_e}{\Delta(\eta_e^2 + \zeta_e^2)^{1/2}}\eta - \frac{\xi_e\zeta_e}{\Delta(\eta_e^2 + \zeta_e^2)^{1/2}}\zeta \,, \\ N &= \frac{\zeta_e}{(\eta_e^2 + \zeta_e^2)^{1/2}}\eta - \frac{\eta_e}{(\eta_e^2 + \zeta_e^2)^{1/2}}\zeta \,. \end{aligned} \tag{B8}$$

With this coordinate system now determined, the projection of a point along a tail axis onto the photographic plane can easily be found. Such a point, found by the method of Appendix A, is denoted by $\xi_{CM},\eta_{CM},0$. Thus the position of this point in L,M,N coordinates is

$$\begin{aligned} L_0 &= \frac{\xi_e}{\Delta}\xi_{CM} + \frac{\eta_e}{\Delta}\eta_{CM} \,, \\ M_0 &= \frac{(\eta_e^2 + \zeta_e^2)^{1/2}}{\Delta}\xi_{CM} - \frac{\xi_e\eta_e}{\Delta(\eta_e^2 + \zeta_e^2)^{1/2}}\eta_{CM} \,, \\ N_0 &= \frac{\zeta_e}{(\eta_e^2 + \zeta_e^2)^{1/2}}\eta_{CM} \,. \end{aligned} \tag{B9}$$

The Earth's position is

$$L_e = \Delta \,, \quad M_e = N_e = 0 \,. \tag{B10}$$

The straight line connecting the Earth and the tail-axis point is

$$\frac{L - L_0}{\Delta - L_0} = -\frac{M - M_0}{M_0} = -\frac{N - N_0}{N_0} \,. \tag{B11}$$

The desired projection of the tail-axis point onto the photographic plane ($L = 0$) is then

$$M_{CM} = M_0 + \frac{M_0 L_0}{\Delta - L_0} \,, \quad N_{CM} = N_0 + \frac{N_0 L_0}{\Delta - L_0} \,, \tag{B12}$$

which, with equations (B9), yields the desired projection of the points ξ_{CM},η_{CM} in the comet orbit plane:

$$\begin{aligned} M_{CM} &= \frac{\Delta}{(\Delta^2 - \xi_e\xi_{CM} - \eta_e\eta_{CM})}\left[(\eta_e^2 + \zeta_e^2)^{1/2}\,\xi_{CM} - \frac{\xi_e\eta_e\eta_{CM}}{(\eta_e^2 + \zeta_e^2)^{1/2}}\right] \,, \\ N_{CM} &= \frac{\zeta_e\Delta^2\eta_{CM}}{(\eta_e^2 + \zeta_e^2)^{1/2}(\Delta^2 - \xi_e\xi_{CM} - \eta_e\eta_{CM})} \,. \end{aligned} \tag{B13}$$

REFERENCES

Alfvén, H. 1957, *Tellus*, **9**, 92.
American Ephemeris and Nautical Almanac (yearly) (Washington, D.C.: Government Printing Office).
Becklin, E. E., and Westphal, J A. 1966, *Ap. J.*, **145**, 445.
Belton, M. J. S. 1965, *A J* , **70**, 451.
———. 1966*a*, in *Nature et origine des comètes* (Rept. 13th Liège Colloq), p. 317.
———. 1966*b*, *Science*, **151**, 35.
Biermann, L., and Trefftz, E. 1964, *Zs. f. Ap* , **59**, 1.
Bobrovnikoff, N. T. 1931, *Pub. Lick Obs.*, **17**, 309.
Brandt, J. C., and Belton, M. J. S. 1966, *Ap. J. Suppl.*, **13**, 125.
Ceplecha, Z. 1958, *Pub. Czech. Astr. Inst.*, **34**, 13.
Finson, M. L , and Probstein, R. F. 1966, AIAA Paper No. 66-32, American Institute of Aeronautics and Astronautics, New York.
Guigay, G 1960, *J. Observateurs*, **43**, 101.
Hayes, W. D., and Probstein, R. F. 1967, *Hypersonic Flow Theory*. Vol, **1**: *Inviscid Flows* (2d ed ; New York: Academic Press).
Hübner, W. F. 1965, *Zs. f. Ap.*, **63**, 22.
Hulst, H. C. van de. 1957, *Light Scattering by Small Particles* (New York: John Wiley & Sons).
Larsson-Leander, G. 1958, *Ark. f. Astr* , **2**, 259.
Liller, W. 1960, *Ap. J.*, **132**, 867.
Miller, F. D. 1961, *Ap. J.*, **134**, 1007.
Ness, N. F., and Donn, B. 1966, in *Nature et origine des comètes* (Rept. 13th Liège Colloq.), p. 343.
Notni, P. 1966, in *Nature et origine des comètes* (Rept. 13th Liège Colloq.), p. 379.
Öpik, E. J. 1958, *Irish A.J.*, **5**, 37.
Osterbrock, D. E. 1958, *Ap. J.*, **128**, 95.
Probstein, R. F. 1968, in *Collection Dedicated to the Sixtieth Birthday of Academician L. I. Sedov*, ed. M. A. Lavrent'ev (Moscow: Izdatel'stvo Akademii Nauk S.S.S.R.) (English ed.: *Problems of Hydrodynamics and Continuum Mechanics* [Philadelphia: Society for Industrial and Applied Mathematics]).
Remy-Battiau, L. 1964, *Bull. cl. sci Acad. roy. Belg*, 5ème sér., **50**, 74.
Roemer, E 1966, in *Nature et origine des comètes* (Rept. 13th Liège Colloq.), p 23
Stefanik, R. P. 1966, in *Nature et origine des comètes* (Rept. 13th Liège Colloq), p. 29.
Sterne, T. E. 1960, *An Introduction to Celestial Mechanics* (New York: Interscience Publishers).
Swings, P. 1965, *Quart. J R.A S.*, **6**, 28.
Vanýsek, V. 1966, in *Nature et origine des comètes* (Rept. 13th Liège Colloq.), p. 255.
Whipple, F. L 1950, *Ap. J.*, **111**, 375.
———. 1951, *Ap. J.*, **113**, 464.
———. 1963, in *The Moon, Meteorites, and Comets*, ed. B. M. Middlehurst and G. P. Kuiper (Chicago: University of Chicago Press), p 639.
Whipple, F. L., and Stefanik, R P. 1966, in *Nature et origine des comètes* (Rept. 13th Liège Colloq.), p 33.
Wurm, K. 1963, in *The Moon, Meteorites, and Comets*, ed. B. M. Middlehurst and G. P. Kuiper (Chicago: University of Chicago Press), p. 573.
———. 1966, in *Nature et origine des comètes* (Rept. 13th Liège Colloq.), p. 119.